Crack Behavior in Asphalt Composite CRCP with Basalt Fiber Reinforcement

Yating Zhang[1] *(corresponding author)*, Zhiyi Huang[2], Jeffery Roesler[3]

Abstract

Basalt fiber-reinforced polymer (BFRP) bars are corrosion-resistant and have potential to be used in continuously reinforced concrete pavements (CRCP). In this paper, the layout of an asphalt composite CRCP test section with BFRP bars at 0.5% is presented. This 8m wide by 250m long, two lane test section has been constructed on G330 National Road in Zhejiang Province, China. A number of instruments, such as temperature sensors and strain gages, were installed to monitor the performance of the test section. An analytical model is introduced to predict the crack behavior of CRCP with BFRP bars compared to conventional CRCP with steel reinforcement. According to the observation before placement of the 10cm asphalt layer, the crack spacing ranged from 3.5m to 5m with crack widths of 1.3mm to 1.4mm, which agreed reasonably well with the predicted values from the analytical model. For similar crack widths as steel-reinforced CRCP, a higher reinforcement ratio is required.

Introduction

Continuously reinforced concrete pavement (CRCP) is a type of high performance pavement structure with closely distributed transverse cracks. The crack width is an important indicator of performance because of its relationship to aggregate interlock and load transfer efficiency between adjacent concrete panels. A study of CRCP in Virginia (McGhee 1974) showed that crack patterns need 2 to 3 years to be fully developed. Various factors that affect the crack width of CRCP were evaluated based on a variety of test sections built in Houston, Texas (Suh and McCullough 1994), which revealed that concrete placed in hotter temperatures develop much wider cracks than those placed in cooler weather and aggregate type and the amount of longitudinal steel has a significant effect on crack widths (Zollinger 1989, 1992). A series of full-scale CRCP accelerated test sections were constructed in Illinois (Kohler and Roesler 2005, 2006), which considered the effects of concrete thickness, steel content, steel depth, and climate on the crack spacing, crack width, and fatigue life of CRCP.

---

[1] Student Member, Ph.D. Candidate, Department of Civil Engineering and Architecture, Zhejiang University, 866 Yuhangtang Ave., Hangzhou, 310058, China, Phone: +1-(217)-904-6825, E-mail: ytzhang666@gmail.com

[2] Ph. D., P. E., Professor, Department of Civil Engineering and Architecture, Zhejiang University, 866 Yuhangtang Ave., Hangzhou, 310058, China, Phone: +86-0571-88208702, E-mail: hzy@zju.edu.cn

[3] Member and Vice President, Ph. D., P. E., Professor, Department of Civil and Environmental Engineering, University of Illinois at Urbana-Champaign, 205 N Mathews Ave., Urbana, IL - 61801 - 2352, USA, Phone: +1- (217)-265-0218, E-mail: jroesler@illinois.edu

Since the early 1990s, hot-mix asphalt (HMA) over CRCP composite pavements were first used for reducing pavement noise in Europe. Later, it was proven that this pavement type not only has good surface characteristics, but also can eliminate transverse reflection cracks in the HMA surface. Based on the main HMA/CRCP test sections in Europe and U.S., it was shown that HMA/CRCP had increased structural and functional performance because of minimal rutting and fatigue damage (Rao et al. 2013). Several HMA/CRCP test sections constructed in the Netherlands and Germany were described in the "2008 Survey of European Composite Pavements" (Tompkins et al. 2010). According to the field data in that report, the overall section condition was excellent, with low noise level from the surface, and there was no transverse reflection cracks on the asphalt surface. Designs for HMA/CRCP to achieve long-life service with low noise and minimum rehabilitation were also developed in the UK (Tompkins et al. 2008). Thin surface course systems were proposed, and several comparison test sections were built to measure the number of transverse reflection cracks in the slab and seasonal thermal movement at the ends of the slabs. The results showed that the asphalt overlay can reduce the temperature differential in the concrete, contributing to less daily and seasonal thermal movement of the concrete cracks.

Recently, new materials such as glass fiber-reinforced polymer (GFRP), a lightweight and corrosion-resistant material, have been used as longitudinal reinforcement in CRCP. The first GFRP-CRCP test section was built in West Virginia, with GFRP as both longitudinal and transverse reinforcement (Chen et al. 2008). An overall design methodology for GFRP-CRCP was proposed based on those test section results (Choi and Chen 2015). Furthermore, an analytical model of a fully-supported reinforced concrete slab was developed to describe the shrinkage and thermal stress distribution in CRCP with GFRP (Chen and Choi 2011). In addition to the analytical model, a finite element model (FEM) was also developed to investigate the performance of CRCP with GFRP, particularly the effects of bar size and concrete aggregates (Eisa et al. 2006). In Canada, a CRCP test section with GFRP, as both longitudinal and transverse reinforcement, was built as an alternative bar type since corrosion of steel is one design criteria for the long service life of CRCP (Benmokrane et al. 2008).

Like GFRP, basalt fiber-reinforced polymer (BFRP), which have great corrosion-resistant characteristics and a high tensile strength, are also a promising alternative for steel in conventional CRCP. Studies in China (Wu 2009, Jiang 2013) have shown the effectiveness of BFRP being used as dowel bars in concrete pavements. The research concerning the effect of different diameters and spacings of BFRP bars on crack spacing and crack width in CRCP were also conducted (Gu et al. 2009). Similar to steel reinforcement, the crack spacing and crack width decreased as the reinforcement ratio increased. Based on the analytical and numerical models, the elastic modulus and bond stiffness of BFRP bars greatly influence the concrete crack width (Ge et al. 2015).

The present study discusses a 250m-long HMA/CRCP composite test section with BFRP that was built in Jinhua, Zhejiang Province (China), to study the early crack behavior of CRCP with BFRP in an HMA/CRCP composite pavement system. The research significance of this work is to evaluate the viability of using BFRP in CRCP sections as well as the reasonableness of the analytical cracking model. An analytical model is presented to predict crack spacing and crack width of BFRP bars in CRCP in order to compare the results to steel reinforcement. Field observations have been conducted both before and after placement of the HMA.

HMA Composite CRCP Project Details

The test section is part of an existing three-lane concrete pavement on G330 National Road at K200+400 to K200+650 (i.e., 250m long test section). Each lane is nominally 4m wide on a 2% longitudinal grade. The two inside lanes were chosen to be part of the test section, which were reconstructed with CRCP containing BFRP bars, while the outer lane was used for thru traffic during reconstruction. After constructing the CRCP section, an HMA layer was placed to form the HMA composite CRCP lanes as well as an HMA overlay on the outer lane's existing, jointed concrete pavement. A longitudinal contraction joint in the 8m wide lane was not part of the design or construction process.

Overview of the test section layout. The construction of the field test section began in September 2014. A cement-stabilized subbase was first constructed with 3% portland cement and crushed stone to provide uniform support. A cement-stabilized base was constructed next on top of the subbase with 5% portland cement and crushed stone. The CRCP thickness was 26 cm with a 6-cm thick HMA binder layer (nominal max aggregate size of 16mm) and a 4 cm thick SBS-modified HMA layer (nominal max aggregate size of 13mm). Between the CRCP and asphalt layer, there is a bonding layer consisting of 1cm-thick SBS-modified asphalt with crushed stone distributed on it. A summary of the composite pavement structure is illustrated in Figure 1.

Figure 1. Zhejiang Test Section with HMA composite CRCP with BFRP bars.

The diameter of longitudinal BFRP bars were 12mm, spaced at 8cm with a reinforcement content of 0.5%, and placed at the mid-depth of concrete slab, i.e., depth of 13cm from surface to top of the bars. The diameter of longitudinal BFRP bars for this CRCP test section were smaller, compared to traditional CRCPs with steel bars. One reason is that the tensile strength of BFRP bars (750MPa) are higher than that of steel bars (550MPa), while the elastic modulus of BFRP bars (40GPa) are closer to concrete (30GPa) than that of steel (210GPa). For this reason, the smaller bar size can be used, without significantly affecting the bond condition between the bars and concrete. The other reason is that BFRP bars are more expensive than the equivalent steel bars, which means using smaller bar size helps reduce the construction cost. Transverse reinforcements were 14mm-diameter BFRP bars, spaced at 50cm and placed at a 30° angle to the horizontal (i.e., skewed), as shown in Figures 2 and 3. The material properties of BFRP bars were obtained from the manufacturer, which are compared to steel bars in Table 1.

Figure 2. Placement of longitudinal BFRP on transverse chairs.

Figure 3. The position of longitudinal and transverse BFRP bars.

Table 1. Geometric and mechanical properties of BFRP and steel reinforcing bars

	Longitudinal BFRP Bars	Transverse BFRP Bars	Typical Steel Bars
Diameter (mm)	12	14	-
Cross-Sectional Area (mm^2)	113.04	153.86	-
Elastic Modulus (GPa)	40	40	210
Tensile Strength (MPa)	750	750	550

For the test section, portland cement, limestone aggregate, and natural sand were used in the concrete mix design with a water/cement ratio of 0.38. The mix design was determined based on the 28-day flexural strength with the concrete properties shown in Table 2. The 28-day shrinkage coefficient and linear expansion coefficient were estimated based on Cao (2001), while others were determined according to Chinese specifications. The 250m concrete slab was cast continuously from 2:00 p.m. to 9:00 a.m., lasting 19 hours, as shown in Figure 4. The ambient humidity and temperature were recorded throughout the construction process (Figure 5).

Table 2. Concrete material properties for CRCP

Modulus of Elasticity (GPa)	Compressive Strength (MPa)	Tensile Strength (MPa)
30	40	3.20
28-day Flexural Strength (MPa)	28-day Coefficient of Shrinkage (mm/mm)	Coefficient of Linear Expansion (/°C)
6.34	0.0002	0.00001

Figure 4. Concrete casting for CRCP with BFRP bars.

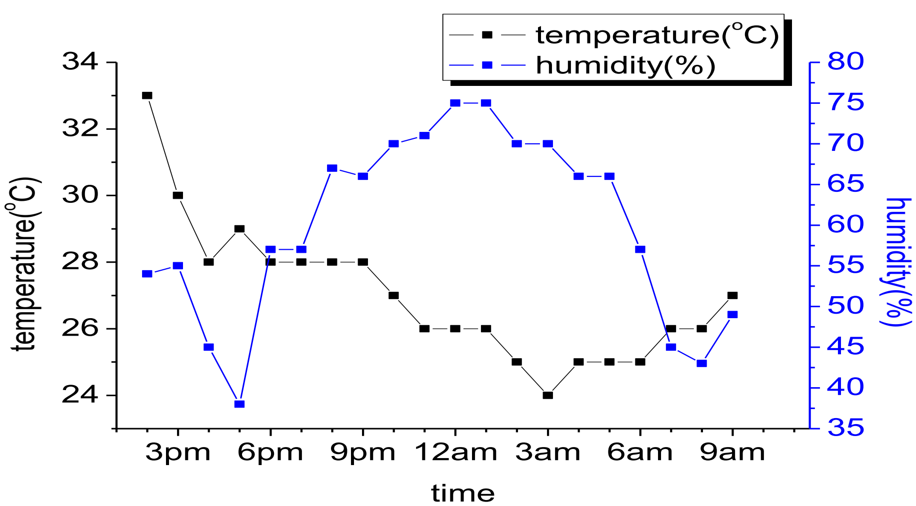

Figure 5. Ambient humidity and temperature during test section construction.

The asphalt overlay was placed one month after casting the CRCP layer. Figures 6 and 7 show the construction of the SMA (SBS-modified asphalt) interlayer above the CRCP layer and the final surface asphalt layer on the test section.

Figure 6. Construction of the SMA interlayer.

Figure 7. Construction of the asphalt overlay.

Temperature sensors and pressure and strain gages were introduced in this test section to monitor the early-age behavior of the CRCP with BFRP bars. Temperature sensors were installed in both the asphalt layer (one at 4cm deep from the asphalt surface and one at the bottom) and concrete layer (one at the top, one at 6cm deep from concrete surface, one at 19cm deep and one at the bottom). Strain gages were placed at the bottom of asphalt layer (three were along the driving direction, two were perpendicular to the driving direction) and concrete layer (one at 6cm deep from concrete surface, one at 19cm deep). Pressure gages were at the bottom of asphalt layer and top of base layer. A remote wireless data collection system was adopted with all results accessed through the internet. The layout of these instruments can be found in Figure 8. Figure 9 shows the data collection system and a sample of the sensors placed in the test section.

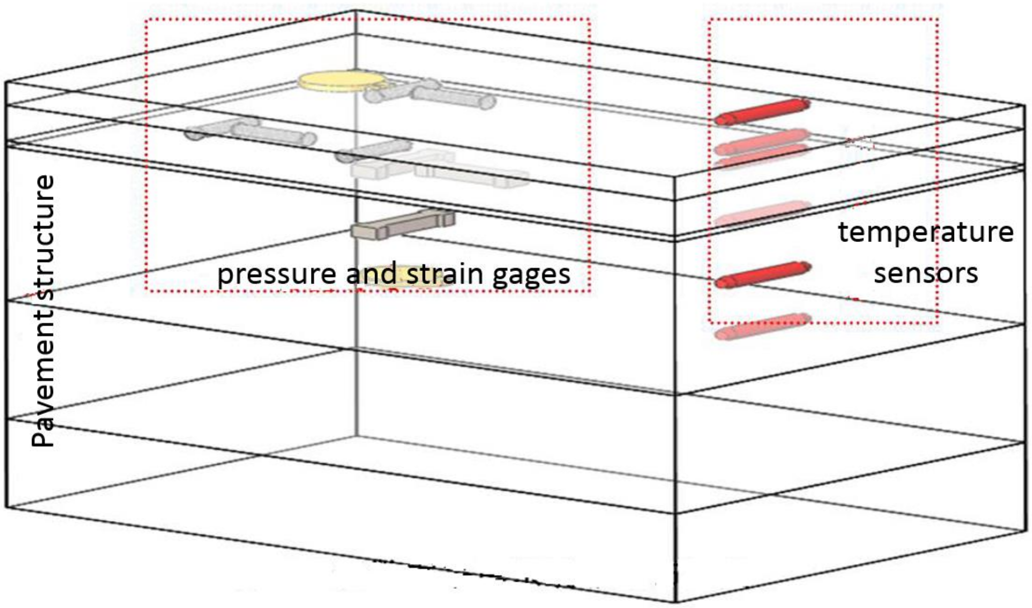

Figure 8. Layout of the installed instruments (yellow ones are pressure gages, grey ones are strain gages and red ones are temperature sensors).

Figure 9. Data collection system and sensors in the CRCP layer.

Analytical model. The friction between the base and the concrete slab imposes a constraint on the concrete horizontal displacement, and thus friction must be introduced into the analytical model to predict crack spacing and crack width (Cao and Hu 2001). It was assumed that the friction-slip relationship between the base and the concrete as well as bond-slip relationship between the reinforcement and the concrete are linear:

$$\tau_c = k_c \cdot u_c \tag{1}$$

$$\tau_s = k_s \cdot (u_c - u_s) \tag{2}$$

where τ_c is frictional stress between base and concrete, τ_s is bond stress between reinforcement and concrete, u_c and u_s are concrete displacement and reinforcement displacement, respectively, k_c is the friction coefficient of concrete slab and base, and k_s is the bond-slip coefficient between concrete and reinforcement. A schematic of the analytical model is shown in Figure 10. Crack spacing and crack width can be calculated with the full derivation of the equations found in Cao (2001).

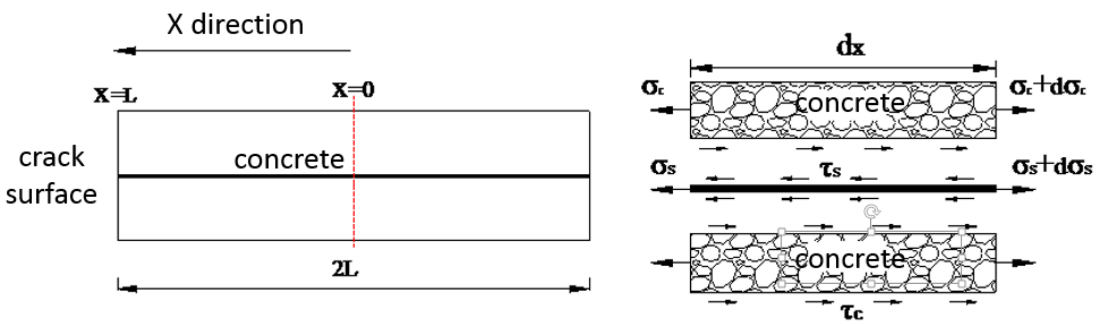

Figure 10. Analytical model for concrete with longitudinal bars (2L is crack spacing).

Based on force equilibrium equations of concrete and reinforcement (3)-(4), and stress-strain relationship of concrete and reinforcement (5)-(6):

$$\frac{d\sigma_s}{dx} + \frac{\pi d_s}{A_c}\tau_s = 0 \tag{3}$$

$$\frac{d\sigma_c}{dx} - \frac{\pi d_s}{A_c}\tau_s - \frac{b}{A_c}\tau_c = 0 \tag{4}$$

$$\sigma_c = E_c \varepsilon_c = E_c\left(\frac{du_c}{dx} + \alpha_c \Delta T + \varepsilon_{sh}\right) \tag{5}$$

$$\sigma_s = E_s \varepsilon_s = E_s\left(\frac{du_s}{dx} + \alpha_s \Delta T\right) \tag{6}$$

where σ_c and σ_s are concrete stress and reinforcement stress, respectively, E_c and E_s are elastic modulus of concrete and reinforcement, respectively, α_c and α_s are the linear expansion coefficients of concrete and reinforcement, respectively, A_c is the cross sectional area of concrete, d_s is reinforcement diameter, b is reinforcement spacing, ε_{sh} is the shrinkage coefficient, ΔT is the mean pavement temperature drop from warmest month to coldest month in the year 2013 in the test section area. Next, u_c and u_s can be expressed in equations (7)-(8):

$$\frac{d^2 u_c}{dx^2} - (a_1 + a_2)u_c + a_1 u_s = 0 \tag{7}$$

$$\frac{d^2u_s}{dx^2} - a_3u_s + a_3u_c = 0 \tag{8}$$

where a_i is indicated below:

$$a_1 = \frac{\pi d_s k_s}{A_c E_c},\ a_2 = \frac{bk_c}{A_c E_c},\ a_3 = \frac{\pi d_s k_s}{A_s E_s}$$

Cao (2001) assumed that the reinforcement displacement and concrete stress are zero at concrete crack surface (x=L), while displacement of both reinforcement and concrete are zero at the mid-slab (x=0). By solving ordinary differential equations at these boundary conditions, u_c and u_s can be calculated in (9) and (10), and σ_c and σ_s can be obtained from equations (11) and (12).

$$u_c = F_1 \sin h(r_1x) + F_2 \sin h(r_3x) \tag{9}$$

$$u_s = F_1b_1 \sin h(r_1x) + F_2b_2 \sin h(r_3x) \tag{10}$$

$$\sigma_c = E_c(F_1r_1 \cos h(r_1x) + F_2r_3 \cos h(r_3x) + \alpha_c\Delta T + \varepsilon_{sh}) \tag{11}$$

$$\sigma_s = E_s(F_1b_1r_1 \cos h(r_1x) + F_2b_2r_3 \cos h(r_3x) + \alpha_s\Delta T) \tag{12}$$

where F_i, r_i, and b_i are defined below:

$$r_1 = \sqrt{\frac{1}{2}[a_1 + a_2 + a_3 + \sqrt{(a_1+a_2+a_3)^2 - 4a_2a_3}]},$$

$$r_3 = \sqrt{\frac{1}{2}[a_1 + a_2 + a_3 - \sqrt{(a_1+a_2+a_3)^2 - 4a_2a_3}]},$$

$$b_1 = (a_1 + a_2 - r_1^2)/a_1,\ b_2 = (a_1 + a_2 - r_3^2)/a_1,$$

$$F_1 = \frac{(\alpha_c\Delta T + \varepsilon_{sh})b_2 \sin h(r_3L)}{b_1r_3 \sin h(r_1L)\cos h(r_3L) - b_2r_1 \cos h(r_1L)\sin h(r_3L)}$$

$$F_2 = \frac{-(\alpha_c\Delta T + \varepsilon_{sh})b_1 \sin h(r_1L)}{b_1r_3 \sin h(r_1L)\cos h(r_3L) - b_2r_1 \cos h(r_1L)\sin h(r_3L)}$$

The final crack spacing (CS) of the CRCP can be obtained by determining the length of CRCP slab that produces an equivalent tensile stress to the concrete tensile strength as seen in equations (13) and (14).

$$\sigma_{c\text{-max}} = \sigma_c|_{x=0} = f_t \tag{13}$$

$$\text{CS} = 2\text{L} \tag{14}$$

where f_t is tensile strength of concrete material. Crack width (CW) can be obtained by knowing this critical slab length from equation (14) and equation (15).

$$\text{CW} = 2u_c\,|_{\text{X=L}} \tag{15}$$

The input parameters used for analytical model predictions are summarized in Table 3. All geometric parameters of concrete and BFRP, i.e. concrete thickness, diameter, and spacing as well as reinforcement content of BFRP, were the same as those specified in the test section. The concrete material properties were the same as those in Table 2. The friction coefficient between concrete and base and linear expansion coefficient of reinforcement were estimated according to Cao (2001), while the bond stiffness of BFRP was calculated through pull-out test results, and ΔT was the mean temperature drop from warmest month to coldest month in the year 2013 in the test section area. To compare the predictions of CRCP with BFRP bars with steel reinforcement in CRCP, all inputs were the same except the bars elastic modulus and tensile strength.

Table 3. Analytical model input parameters for CRCP test section

	Concrete	BFRP	Steel
Modulus of Elasticity (GPa)	30	40	210
Tensile Strength (MPa)	3.20	750	550
Compressive Strength (MPa)	40	-	-
Coefficient of Shrinkage	0.0002	-	-
Coefficient of Linear Expansion (/˚C)	0.00001	0.000009	0.000009
Thickness of Concrete (cm)	26	-	-
Reinforcement Content (%)		0.50	0.50
ΔT (℃): 30	-	-	-
Friction Coefficient (MPa/m)	40	-	-
Bond Stiffness (GPa)	-	30	30
Diameter (mm)	-	12	12
BFRP Spacing (cm)	-	8	8

Figure 11 shows the analytical prediction results for CRCP with BFRP or steel bars. When the concrete stress reached its tensile strength (3.2MPa), the concrete was assumed to produce a transverse crack and a certain crack width. For the CRCP with BFRP model parameters, CS and CW were 4.47m and 1.78mm, respectively, while for CRCP with steel, CS and CW were 2.01m and 0.82mm. The larger crack spacing and width for the BFRP is because of its lower elastic modulus (40GPa) as compared to steel (210GPa). For this comparison, the stress in the steel exceeded 75% of the yield strength so a larger bar diameter or higher steel content would theoretically be needed for a fairer comparison. In order to achieve lower CS and CW in the CRCP with BFRP, the reinforcement ratio needs to be increased.

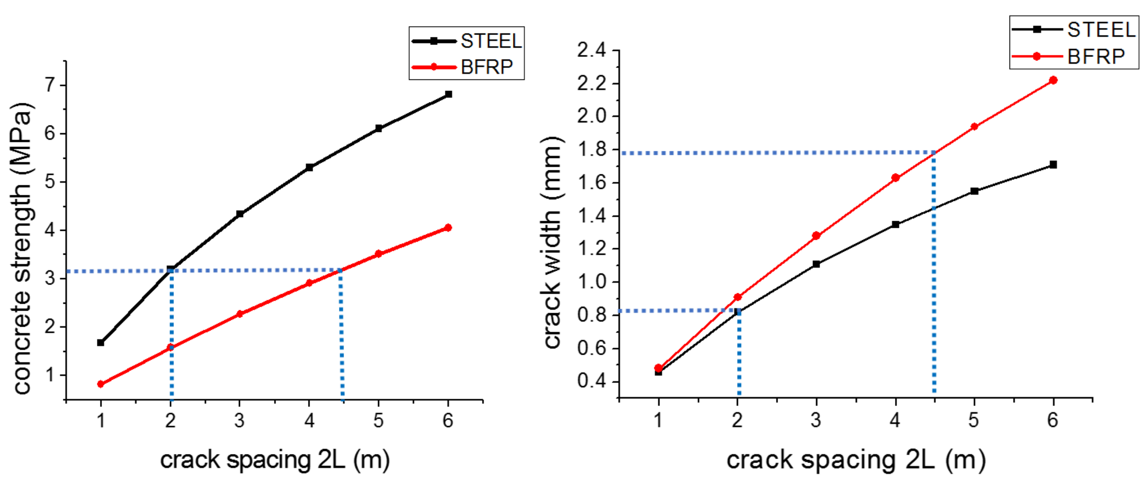

Figure 11. Predictions of crack spacing and crack width for steel and BFRP.

Field observation of cracks. Three crack surveys were performed during the first month, before placement of the final asphalt surface. The first survey occurred at about 12 hours after slab casting. The second observation was the 12th day after casting, and the final survey was conducted 36 days after concrete placement. Based on test section observations, almost all of the cracks were transverse to the direction of travel (Figure 12), except for one longitudinal crack, which was 11m long at the end of the test section (Figure 13). The observational records of the crack surveys are shown in Table 4.

Figure 12. Typical transverse cracks in the CRCP section.

Figure 13. Longitudinal crack at the end of the test section.

Table 4. Observation records of CRCP with BFRP test section

	First	Second	Third
Time	12 hours after slab casting	12 days after casting	36 days after casting
Transverse crack spacing	Only one crack near the end of the slab	Many transverse cracks; all crack spacings were between 4m and 7m.	New cracks appeared between existing transverse cracks; new crack spacing developed to 3.5m-5m
Transverse crack widths	Around 0.4mm	Around 1mm (mean value)	Widths of new cracks were around 0.2mm, while the widths of existing cracks were 1.3mm-1.4mm (see Figure 14)
Longitudinal cracks	No crack	One 11m-long longitudinal crack	Same 11m-long crack, but irregular cracks appeared (see Figure 15)

Figure 14. Transverse crack width of initial crack.

Figure 15. Irregular cracks at the end of the test section.

The longitudinal and other irregular cracks likely developed because no longitudinal contraction joint was sawn to split the 8m lane into a more conventional lane width of 4m. As for crack width, the new transverse cracks appearing on the third survey were lower compared to existing transverse cracks because of the greater concrete stiffness at later ages and shorter spacing between cracks. Figure 16 shows the position of cracks generated in the whole test section, including both transverse cracks and irregular cracks.

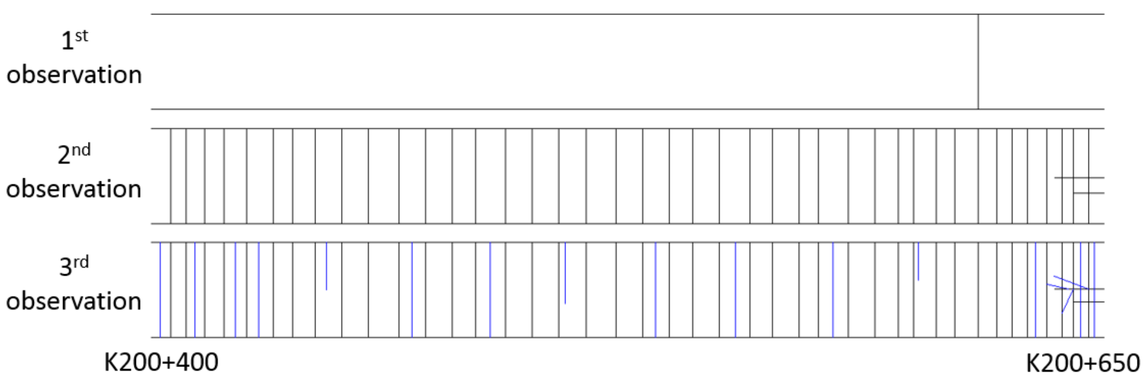

Figure 16. Crack maps of test section from observational surveys.

After finishing the asphalt overlay, a field observation was conducted on December 14 (98 days after slab casting and 61 days after placement of the HMA overlay). The HMA composite CRCP test section showed no transverse cracks except for the one at the end of the test section (Figure 17), where irregular cracks had appeared in the CRCP before placing the asphalt layer. In addition to the transverse crack, there is a longitudinal reflection crack in the HMA at the construction joint between the new CRCP lanes and existing JPCP, as shown in Figure 18. The irregular crack at the end of the concrete slab is likely responsible for the transverse reflection crack shown in the HMA. The appearance of the longitudinal reflection crack is because of the differential deflection at the construction joint between the newly constructed CRCP and the existing JPCP.

Figure 17. Transverse reflection crack in the HMA.

Figure 18. Longitudinal reflection crack in the HMA.

Comparison and analysis. Table 5 summarizes the crack spacing and crack width results of CRCP with BFRP bars without asphalt overlay, according to field observation and analytical calculation.

Table 5. Comparison of actual and predicted crack spacing and crack width

	Crack spacing	Crack width
Final field observation	from 3.5m to 5m	from 1.3mm to 1.4mm
Analytical results	4.47m	1.78mm

As for crack spacing, the results of analytical calculation was 4.47m, which is in the range of 3.5m to 5m and consistent with field observation results. For crack width, the analytical result was 1.78mm, which is a little higher than field observation (1.3mm-1.4mm). This difference is linked to the linear bond-slip assumption between the reinforcement and concrete, concrete slab to base friction model, and differential moisture and temperature effects in the field that are not included in the model. Furthermore, the ΔT assumed in the analytical model is higher than the actual temperature drop between the maximum and minimum (mean) temperature for the first 36 days after casting concrete (3^{rd} visual survey). Therefore, a reasonable agreement was achieved from field observation and analytical calculation for crack spacing and slight overprediction of crack width at earlier ages occurred with the model.

Conclusions

BFRP bars are currently available and have potential to be used in CRCP. The elastic modulus of the BFRP is significantly less than steel, and thus, concerns over the developing crack spacing and crack width are valid, given typical reinforcement ratios for CRCP. A 250m test section of HMA composite CRCP with BFRP bars was constructed in Zhejiang Province, China. Crack spacing in the test section after one month was measured prior to placement of the HMA overlay and found to be 3.5m to 5m with crack widths at the surface of 1.3mm to 1.4mm. An analytical model was presented to predict the crack behavior, with the crack spacing and width of 4.47m and 1.78mm, respectively, reasonably agreeing with the visual survey results for crack spacing but overpredicting for crack width. Only one transverse reflection crack and one longitudinal crack were seen on the asphalt surface (98 days after slab casting and 61 days after placement of the HMA overlay), which were located at the end of test section. Further field observations of this test section are still necessary, and load transfer efficiency between adjacent slabs with BFRP bars needs to be conducted because of the larger crack width compared to conventional CRCP with steel.

Acknowledgements
This project was funded by China Department of Transportation. The test section was built with the support of Transportation Research Institute in Zhejiang Province, contractors, and Zhejiang University researchers.

References
Benmokrane, B., Eisa, M., et al. (2008). "First Use of GFRP Bars as Reinforcement for Continuous Reinforced Concrete Pavement." *Proc., Fourth International Conference on FRP Composites in Civil Engineering,* Zurich, Switzerland.

Cao, D. (2001). "Research on Continuously Reinforced Concrete Pavement Structure." *Ph. D. Thesis,* Chang'an University, Xi'an, China.

Cao, D., and Hu, C. (2001). "An Analysis of Thermal Stress in Continuously Reinforced Concrete Pavement." *Journal of Xi'an Highway University,* 21(2), 1-4.

Chen, H. L., Choi, J. H., GangaRao, H. V., and Kopac, P. A. (2008). "Steel versus GFRP Rebars?" *Public Roads*, 72(2), 2–10.

Chen, R. H. L., and Choi, J.-H. (2011). "Analysis of Shrinkage and Thermal Stresses in Concrete Slabs Reinforced with GFRP Rebars." *Journal of Materials in Civil Enginnering,* 23(5), 612-627.

Choi, J.-H., and Chen, R. H. L. (2015). "Design of GFRP Reinforced CRCP and its Behavior Sensitivity to Material Property Variations." *Construction and Building Materials*, 79, 420-432.

Eisa, M., EI-Salakawy, E. F., and Benmokrane, B. (2006). "Finite Element Model for New Continuous Reinforced Concrete Pavement (CRCP) using GFRP Bars." *Proceedings, 17th International Conference on Modelling and Simulation*, Montreal, Quebec, Canada, 609-616.

Ge, Q. et al. (2015). "The Design of BFRP in Asphalt Composite CRCP." *Journal of Zhejiang University (Engineering Science),* 49(1), 1-7.

Gu, X., Lu, J., and Shen, X. (2009). "Research on Reinforcement Design in BFRP-CRCP." *Highway Traffic Science and Technology,* 53(5), 33-36.

Hassan, K. E. et al. (2008). "Durability of Continuously Reinforced Concrete Surfaced with Asphalt." *TRL Report TRL666,* http://www.trl.co.uk, United Kingdom.

Jiang, S. (2013). “The Application of BFRP in Concrete Pavement.” *Master Thesis,* Dalian Maritime University, Dalian, China.

Kohler, E. and Roesler, J. (2006), Accelerated Pavement Testing of Extended Life Continuously Reinforced Concrete Pavement Sections, Final Report, *Transportation Engineering Series No. 141*, *Illinois Cooperative Highway and Transportation Series No. 289*, University of Illinois, Urbana, IL, 354 pp.

Kohler, E., and Roesler, J. (2005). “Crack Width Measurements in Continuously Reinforced Concrete Pavements.” *Journal of Transportation Engineering*, 131(9), 645-652.

McGhee, K. H. (1974). “Experience with Continuously Reinforced Concrete Pavements in Virginia.” *Transportation Research Record,* 485, 14-24.

Rao, S., Darter, M., and Tompkins, D., et al. (2013). “SHRP 2 Report S2-R21-RR-2-Composite Pavement Systems.” *Transportation Research Board,* Washington, D.C.

Suh, Y-C, and McCullough, B. F. (1994). “Factors Affecting Crack Width of Continuously Reinforced Concrete Pavement.” *Transportation Research Record*, 1449, 134-140.

Tompkins, D., et al. (2010). “SHRP 2 Report S2-R21-RW-1-2008 Survey of European Composite Pavements.” *Transportation Research Board,* Washington, D.C.

Wu, F. (2009). “The Study of Bond-Slip Relationship between BFRP and Concrete.” *Master Thesis,* Dalian University of Technology, Dalian, China.

Xin, D., Zollinger, D., and James, R. (1992). “One-Dimensional Model for Analysis of CRC Pavement Growth.” *Journal of Transportation Engineering*, 118(4), 557-575.

Zollinger, D. (1989). “Investigation of Punchout Distress in Continuously Reinforced Concrete Pavement.” *Ph.D. Thesis,* University of Illinois, Urbana, IL, USA.